

## Article

# The Influence of Raw Materials on the Stability of Grisaille Paint Layers

Carla Machado <sup>1,2,\*</sup> , Márcia Vilarigues <sup>1,2</sup> , Joana Vaz Pinto <sup>3</sup>  and Teresa Palomar <sup>2,4,\*</sup> 

<sup>1</sup> Department of Conservation and Restoration, NOVA School of Science and Technology, 2829-516 Caparica, Portugal

<sup>2</sup> Research Unit VICARTE–Glass and Ceramics for the Arts, NOVA School of Science and Technology, 2829-516 Caparica, Portugal

<sup>3</sup> CENIMAT I3N, Department of Materials Science and CEMOP/UNINOVA, NOVA School of Science and Technology, 2829-516 Caparica, Portugal

<sup>4</sup> Institute of Ceramic and Glass, Spanish National Research Council (ICV-CSIC), 28049 Madrid, Spain

\* Correspondence: cf.machado@campus.fct.unl.pt (C.M.); t.palomar@csic.es (T.P.)

**Abstract:** Grisaille is a glass-based paint made by mixing metal oxides (iron or copper) with ground lead-silica glass. The different materials used in the grisailles production (coloring agents, base glasses, or vehicles) can significantly impact their long-term stability along with the firing conditions. The main objective of this study was to achieve a better understanding of how raw materials influence the production and stability of these paints. To achieve this goal, 27 grisailles were produced, changing the raw materials, proportions, and firing conditions. The produced grisailles were characterized by X-ray fluorescence and diffraction, colorimetry, roughness measurement, and contact angle analysis. Adhesion and cleaning tests were also made. The use of different coloring agents has a significant impact on the final appearance and on the chemical and mechanical stability of the grisailles, but the latest is more affected by both firing temperature and the proportion between pigments and base glasses.

**Keywords:** grisaille; recipe; raw material; conservation; degradation



**Citation:** Machado, C.; Vilarigues, M.; Pinto, J.V.; Palomar, T. The Influence of Raw Materials on the Stability of Grisaille Paint Layers. *Appl. Sci.* **2022**, *12*, 10515. <https://doi.org/10.3390/app122010515>

Academic Editor: Claudia Mondelli

Received: 16 August 2022

Accepted: 14 October 2022

Published: 18 October 2022

**Publisher's Note:** MDPI stays neutral with regard to jurisdictional claims in published maps and institutional affiliations.



**Copyright:** © 2022 by the authors. Licensee MDPI, Basel, Switzerland. This article is an open access article distributed under the terms and conditions of the Creative Commons Attribution (CC BY) license (<https://creativecommons.org/licenses/by/4.0/>).

## 1. Introduction

Grisaille was the first glass-based paint to be used in stained-glass windows. Its use spread throughout Europe from the 12th century onwards and is still used today for drawing the contours and outlines of images, called *grisaille à contourner*, and for the creation of shadows and textures, *grisaille à modéler* [1–4]. The grisailles are usually dark in color, mainly in different shades of brown and black, and are painted on colored or colorless glass supports, together with enamels, sanguine paint, and yellow silver stain [1].

The production of grisailles has changed slightly throughout history, being the first known grisaille recipe found in the Eraclius manuscript “*De coloribus et artibus Romanorum*” (10th–13th century). He describes the paint as a mixture of iron pieces that fall from the blacksmith anvil (oxidized iron) with Jewish glass (ground lead-rich silicate glass) [2,5]. This mixture of base glass and coloring agents is painted on a glass support and fired at temperatures between 650 °C and 700 °C. After the firing process, a thin and uneven layer of colorless glass matrix with the iron oxides dispersed is formed [4]. Recipes for grisaille paint can be found in historical written sources from the 10th to the 19th century [2]. The most common raw materials identified were base glasses and coloring agents [2]. The first ones permit the grisaille adhesion to the glass support and the second ones are responsible for the grisaille coloration.

The use of a high lead base glass continued to be described throughout the different sources, slightly varying the proportions between the silica and lead oxide or even changing the lead source in their production [2]. Initially, it is mainly described the use of burned lead,

for example, in the Eraclius recipe for the Jewish glass [5], and later, as in the 19th-century treatise *Guide du verrier* by Georges Bontemps, is described the use of the mineral minium as lead source [6]. The lead is going to reduce the melting temperature of the glass [7], which explains the continuous use of high lead-based glasses in the grisailles formulation, as it is needed that grisailles have a lower melting temperature than the support glass in the way of not deforming it during the firing treatment of the paint layer.

Iron and/or copper oxides, obtained by firing these two metals, were the main coloring agents described throughout the centuries [2,4]. However, firstly proposed by Vasari in the 16th century [8] and later described by Bontemps [6], iron-based pigments, such as hematite, substituted these burned metals. Manganese is also punctually mentioned as a grisaille colorant in the 17th century, *Ars Vitrarum Experimentalis* by Johannes Kunckel.

The recipes also describe vehicles and temporary binding agents as the materials that give the necessary plasticity to the mixture before being fired, allowing it to be applied on the glass support. The vehicles usually described are the common ones used in glass painting, such as gum arabic and water, wine, vinegar, egg white, and oils such as lavender oil [2].

Other materials, including various compounds, are also mentioned. The role of these compounds on the grisailles is uncertain, as it is not described in the historical sources. However, they can be understood as additives that can work as opacifiers and/or fluxes. For example, the use of the pigment lead white, described by Kunckel, can also help lower the melting temperature [2].

From the analytical results on historical grisaille compositions described in the literature, it was possible to confirm the use of the same raw materials described in the historical recipes. The grisailles generally present a high quantity of lead in their composition [9–11], which confirms the use of high lead-based glass in their production. Veritá et al. [12] analyzed the stained-glass windows of the Sainte Chapelle in Paris (France) and detected that the vitrified matrix had high lead contents, low silica, and small traces of alumina, lime, and potash [12]. Regarding the coloring agents, it is also possible to confirm the recurrent use of iron and copper oxide, being the hematite ( $\alpha\text{-Fe}_2\text{O}_3$ ) and tenorite (CuO), the main compounds identified in historical grisailles used individually or in combination, agreeing with the historical recipes [9,11,13]. When used in combination, mixed compounds can be formed as the cuprospinel ( $\text{CuFe}_2\text{O}_4$ ), identified in the grisailles from the cathedral of St. Michael and Gudule in Brussels (Belgium) [14] and in the grisailles from the cathedrals of Avila and Segovia (Spain) [11].

All the changes in the raw materials can impact the grisaille paint layer's stability. As stated by Bettembourg [8] and further developed by others [1,9], the grisaille alteration can depend on its chemical composition and production methodology. Additionally, the firing conditions, the ratios between the different components, and the compatibility between the grisaille and the substrate glass can also influence the grisaille's durability [1,15,16]. For example, Schalm et al. [14] proposed that the pulverization of the granular grisailles from the windows of the cathedral of St. Michael and St. Gudule in Brussels (Belgium) is probably due to an unbalanced proportion between the coloring agents and base glass, which can lead to a poor attachment of the pigment grains to the glass support that can easily result in paint loss with small mechanical stress [1,14].

Hence, this work aims to understand better how raw materials and different production methodologies can influence the long-term conservation and stability of grisaille paint layers.

## 2. Materials and Methods

### 2.1. Samples Preparation

To better understand the influence of the raw materials on the stability, different grisailles were produced and compared, changing one variable each time, showed in Table 1. The variables considered were the coloring agents, base glass, vehicles and other materials, the firing temperature, the proportions between the components, and the glass support (Table 1).

**Table 1.** Produced grisailles formulation and image of the final grisaille for each formulation. (\* grinding time, PA: practical grade).




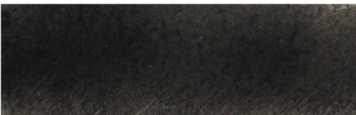
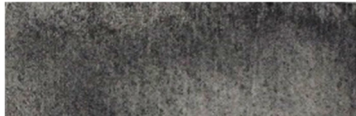
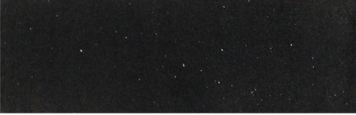

Variables	Coloring Agents (CA)	Base Glass (BG)	(CA:BG) wt%	Vehicle	Other Materials	Substrate Glass	Temp.	Image of Final Grisaille
Model grisaille	Iron and copper (1:1 wt%)	Rocaille (SiO <sub>2</sub> + PbO (1:3 wt%))	(1:1)	Gum arabic + water	-	Glass slide	650 °C	
Coloring agents	Burned iron (10 min *)	Rocaille	(1:1)	Gum arabic + water	-	Glass slide	650 °C	
	Burned iron (5 min *)	Rocaille	(1:1)	Gum arabic + water	-	Glass slide	650 °C	
	Burned copper (10 min *)	Rocaille	(1:1)	Gum arabic + water	-	Glass slide	650 °C	
	Burned copper (5 min *)	Rocaille	(1:1)	Gum arabic + water	-	Glass slide	650 °C	
	Manganese (PA MnO <sub>2</sub> )	Rocaille	(1:1)	Gum arabic + water	-	Glass slide	650 °C	
	Hematite (PA Fe <sub>2</sub> O <sub>3</sub> )	Rocaille	(1:1)	Gum arabic + water	-	Glass slide	650 °C	

Table 1. Cont.

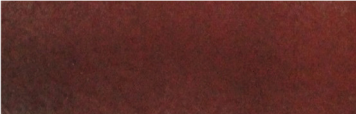
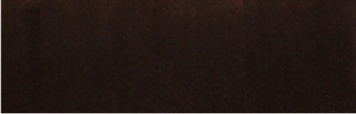



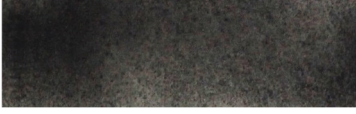
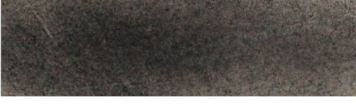
Variables	Coloring Agents (CA)	Base Glass (BG)	(CA:BG) wt%	Vehicle	Other Materials	Substrate Glass	Temp.	Image of Final Grisaille
	Hematite (mineral)	Rocaille	(1:1)	Gum arabic + water	-	Glass slide	650 °C	
	Burned umber (pigment)	Rocaille	(1:1)	Gum arabic + water	-	Glass slide	650 °C	
Base glass	Iron and copper (1:1 wt%)	SiO <sub>2</sub> + PbO (1:2 wt%)	(1:1)	Gum arabic + water	-	Glass slide	650 °C	
	Iron and copper (1:1 wt%)	SiO <sub>2</sub> + PbO (1:4 wt%)	(1:1)	Gum arabic + water	-	Glass slide	650 °C	
Vehicles	Iron and copper (1:1 wt%)	Rocaille	(1:1)	Water	-	Glass slide	650 °C	
	Iron and copper (1:1 wt%)	Rocaille	(1:1)	Urine	-	Glass slide	650 °C	
	Iron and copper (1:1 wt%)	Rocaille	(1:1)	Wine	-	Glass slide	650 °C	

Table 1. Cont.





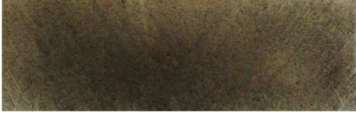
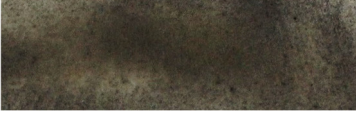
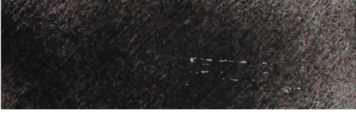


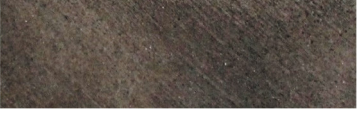
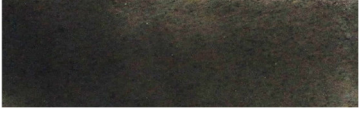
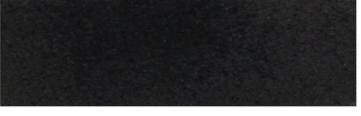
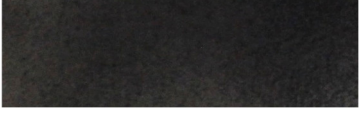
Variables	Coloring Agents (CA)	Base Glass (BG)	(CA:BG) wt%	Vehicle	Other Materials	Substrate Glass	Temp.	Image of Final Grisaille
	Iron and copper (1:1 wt%)	Rocaille	(1:1)	Vinegar	-	Glass slide	650 °C	
Other materials	Iron and copper (1:1 wt%)	Rocaille	(1:1)	Gum arabic + water	Alumina (PA Al <sub>2</sub> O <sub>3</sub> )	Glass slide	650 °C	
	Iron and copper (1:1 wt%)	Rocaille	(1:1)	Gum arabic + water	Antimony (PA Sb <sub>2</sub> O <sub>3</sub> )	Glass slide	650 °C	
	Iron and copper (1:1 wt%)	Rocaille	(1:1)	Gum arabic + water	Burned lead and tin (Pb <sub>2</sub> SnO <sub>4</sub> )	Glass slide	650 °C	
	Iron and copper (1:1 wt%)	Rocaille	(1:1)	Gum arabic + water	Burned lead (PA PbO)	Glass slide	650 °C	
	Iron and copper (1:1 wt%)	Rocaille	(1:1)	Gum arabic + water	Lead white (2PbCO <sub>3</sub> ·Pb(OH) <sub>2</sub> )	Glass slide	650 °C	
Temperature	Iron and copper (1:1 wt%)	Rocaille	(1:1)	Gum arabic + water	-	Glass slide	600 °C	

Table 1. Cont.

Variables	Coloring Agents (CA)	Base Glass (BG)	(CA:BG) wt%	Vehicle	Other Materials	Substrate Glass	Temp.	Image of Final Grisaille
CA:BG	Iron and copper (1:1 wt%)	Rocaille	(1:1)	Gum arabic + water	-	Glass slide	700 °C	
	Iron and copper (1:1 wt %)	Rocaille	(2:1)	Gum arabic + water	-	Glass slide	650 °C	
	Iron and copper (1:1 wt%)	Rocaille	(1:2)	Gum arabic + water	-	Glass slide	650 °C	
Substrate glasses	Iron and copper (1:1 wt%)	Rocaille	(1:1)	Gum arabic + water	-	Mixed-alkali glass (K-Na-Ca-Si)	650 °C	
	Iron and copper (1:1 wt%)	Rocaille	(1:1)	Gum arabic + water	-	Soda-lime glass (Na-Ca-Si)	650 °C	
	Iron and copper (1:1 wt%)	Rocaille	(1:1)	Gum arabic + water	-	Potash-lime glass (K-Ca-Si)	650 °C	

The initial grisaille (Model grisaille) formulation agrees with the most common raw materials identified in the historical treatises [2]. It was made by mixing burned iron and burned copper (1:1 wt%) as coloring agents, rocaille ( $\text{SiO}_2 + \text{PbO}$  (1:3 wt%)) as base glass, gum arabic (0.1 wt%) and water as temporary binder and vehicle. The base glass and the coloring agents were used in a 1:1 wt% ratio, painted on the non-tin side of commercial glass slides (Deltalab<sup>®</sup>), following the paint application methodology from Vilarigues et al. [3], and fired at 650 °C. A total of 26 grisailles were produced, changing one of the variables each time (see Table 1).

Practical grade (PA) reagents were used for some raw materials. All the brands and manufacturers of the commercial PA reagents are described in Appendix A.

Low-carbon steel and standard copper plates were used to obtain the burned iron and copper. Both metals were cut into small pieces and placed in crucibles in an electric furnace, during two heating cycles, to a maximum temperature of 850 °C for 1 h, promoting metal oxidation. Afterward, both metals were grounded into a fine powder for 5 and 10 min.

The  $\text{SiO}_2$  and  $\text{PbO}$  for the base glasses were mixed in different proportions (Table 1). After 10 h of melting in an electric furnace (BARRACHA-model E6) at 1100 °C in ceramic crucibles, the mixtures were poured into water, dried, and grounded in an electric agate mortar.

Different substrate glasses were produced (Table 1) according to the compositions of the most common glasses from historical stained-glass windows [17]. They were melted in an electric furnace (TERMOLAB-BL) at 1400 °C for 3.5 h in ceramic crucibles and blown into the form of a roundel using the same procedure as the historical production of crown-window glass.

Most of the other materials added were practical grade reagents, except for the burned tin and lead and the lead white. The burned tin and lead were produced according to the descriptions from historical recipes; lead oxide ( $\text{PbO}$ ) and tin oxide ( $\text{SnO}_2$ ) were mixed in a 1:1 wt% ratio and burned at 900 °C for 2 h. This burned lead and tin was also known as a lead-tin-yellow pigment, widely used in oil painting [18].

The lead white pigment used was produced by exposing metallic lead to acetic acid (vinegar) [18].

The other materials (alumina, antimony, burned lead and tin, burned lead, and lead white) were added to the grisailles in proportions of 1:1 wt% with the coloring agents. Moreover, the sum of the coloring agents and the other materials was 1:1 wt% with the base glass. Leaving grisailles with 1:1:2 wt% proportions between the coloring agents, other materials, and base glasses. These ratios were chosen according to the quantities described in the historical recipes with these materials in their composition [2].

The different grisaille mixtures were painted and fired at different temperatures (600 °C, 650 °C, 700 °C) in a side-heated electric furnace (BARRACHA-model E1) with a temperature ramp of 3 °C/min up to the maximum temperature, followed by a dwell of 30 min and slow cooling. All the produced grisailles are shown in Table 1.

## 2.2. Analytical Techniques

The raw materials were characterized by X-ray fluorescence and X-ray diffraction. The produced grisailles were also characterized by X-ray diffraction, and the roughness, contact angle, and color were measured. Adhesion tests were conducted to assess the grisaille adhesion to the glass substrate. The tests were performed following the *European ISO Standard, Paints, and varnishes—Cross-cut test* (ISO 2409:1992). Following Wolbers' methods [11], a cleaning study was also performed to test the chemical solubility of these grisailles.

To identify the chemical composition of the different base and substrate glasses used in the sample preparation, analyses by X-ray fluorescence (XRF) were made. A PANalytical MagicX (PW-2424) wavelength-dispersed X-ray spectrometer equipped with a rhodium tube (SUPER SHARP) of 2.4 KW was used. Analytical determinations were carried out through the analysis of the  $\text{IQ}^+$  curve, with a powder sample prepared in a fused pearl. The pearls were made in a Philips Perl'X3 equipment, melted at 1050 °C, in a platinum-gold

crucible, from a homogeneous mixture of 0.3 g of the powder sample (<75  $\mu\text{m}$ ) and 5.5 g of  $\text{Li}_2\text{B}_4\text{O}_7$  anhydrous and LiBr. The spectrometer can detect light elements starting at 18.998 atomic mass (Fluor) with an LOD of 0.1%.

The X-ray diffraction (XRD) of the coloring agents and additives identified the different crystallographic phases of the compounds. A Benchtop X-Ray Diffractometer RIGAKU model MiniFlex II, with a monochromatic X-ray source (Cu K $\alpha$  line) operated at 30 kV of acceleration voltage and 15 mA current, was used. The spectra were acquired between 10 and 90° at 2°/min. X-ray diffraction was also performed on selected grisaille samples to identify the different crystallographic phases formed after the firing. A PANalytical X'Pert PRO MPD diffractometer equipped with an X'Celerator 1D detector and CuK $\alpha$  radiation was used. The XRD data were acquired in the 14°–90° 2 $\theta$  range with a step size of 0.02°. The identification was made using the X'Pert HighScore Plus software and database and by comparison with the RRUFF database.

Roughness analyses were performed to compare and measure the surface morphology of the samples. The measurements were made with an optic rugosimeter TRACEiT from Innowep GmbH. Three-dimensional topographical maps (5  $\times$  5 mm) with a resolution of 2.5  $\mu\text{m}$  (Z-axis) and 2.5  $\mu\text{m}$  (in X/Y axes). To compare the samples, the roughness maps were flattened, and the arithmetic average roughness (Ra) was measured with the software Gwyddion version 2.6 [19] and calculated following the method of Ariyathilaka et al. [20]

Contact angle measurements were made to attest to the hydrophilic and hydrophobic properties of the samples. Under laboratory conditions, the tests were performed using distilled water with the Easy Drop Standard “Drop Shape Analysis System” Kruss DSA 100 measurement apparatus. The diameter of the needle was 0.5 mm, and the drop volume was 2  $\mu\text{L}$ . The contact angle of each sample was measured automatically by the equipment in the fitting mode three times, and the average and standard deviation were calculated.

A colorimetric study was performed to measure the color variations between the samples. A CM-700d Konica Minolta portable sphere spectrophotometer with vertical alignment with an 8 mm diameter mask was used. The data were recorded in SCI mode with a D65 Illuminant and processed by Color Data Software CM-1 in a CIELab color space. The analyses were performed in three areas on each sample, calculating the averages and standard deviation. Afterward, the results were converted to xy coordinates, and the results were expressed in a chromaticity diagram CIE 1931.

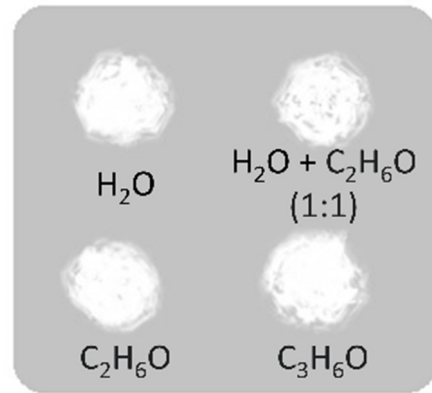
Finally, it was assessed the adhesion of the grisaille to the glass substrate by adhesion tests. Following the *European ISO Standard, Paints, and varnishes—Cross-cut test* (ISO 2409:1992) [21]. An Elcometer<sup>®</sup> cutter with six blades (equally spaced by 1 mm) was used, and the ISO Standard Adhesive Tape was applied. The test was performed three times in each sample to verify the uniformity samples and the reproducibility tests. Based on the Classification Table for the ISO Standard [21], the results were classified from 0 to 5, corresponding to:

- 0—Only the superficial layer was cut without detachment;
- 1—Only the superficial layer was cut, with residual detachment visualized in the adhesive tape;
- 2—Residual detachment was visualized in the adhesive tape, and between 5% and 15% of the cross-cut area was affected;
- 3—Residual detachment was visualized in the adhesive tape at 15%, and 35% of the cross-cut area was affected;
- 4—Residual detachment was visualized in the adhesive tape at 35%, and 65% of the cross-cut area was affected;
- 5—Total detachment of the painted layer.

A cleaning study was made on the studied samples to test their solubility and solvent resistance. The methodology for this cleaning study was adapted from Wolbers' methods for painted surfaces of temperas and oils [22]. The solubility was evaluated with four solutions: distilled water ( $\text{H}_2\text{O}$ ), distilled water ( $\text{H}_2\text{O}$ ) + ethanol ( $\text{C}_2\text{H}_6\text{O}$ ) (1:1), ethanol ( $\text{C}_2\text{H}_6\text{O}$ ), and acetone ( $\text{C}_3\text{H}_6\text{O}$ ). These solutions are the most common ones used



for cleaning stained-glass windows [23]. The samples' surfaces were cleaned with each solution (Figure 1) under the observation of the Dino-Lite Edge digital portable microscope, model AM7915MZTL.



**Figure 1.** Representation of the order and position in which the solvents were tested in the sample cleaning study.

### 3. Results and Discussion

#### 3.1. Raw Materials Characterization

The chemical composition of base and substrate glasses was analyzed by X-ray fluorescence, as shown in Tables 2 and 3.

**Table 2.** Base glasses composition (wt.%) obtained by XRF.

	Na <sub>2</sub> O	Al <sub>2</sub> O <sub>3</sub>	SiO <sub>2</sub>	K <sub>2</sub> O	Fe <sub>2</sub> O <sub>3</sub>	PbO
SiO <sub>2</sub> :PbO (1:2)	-	0.57	33.9	-	-	65.5
SiO <sub>2</sub> :PbO (1:3)	-	1.97	26.7	-	-	71.3
SiO <sub>2</sub> :PbO (1:4)	0.56	2.26	28.6	0.15	0.22	68.0

**Table 3.** Substrate glasses composition (wt.%) obtained by XRF.

	Na <sub>2</sub> O	MgO	Al <sub>2</sub> O <sub>3</sub>	SiO <sub>2</sub>	P <sub>2</sub> O <sub>5</sub>	K <sub>2</sub> O	CaO	MnO	Fe <sub>2</sub> O <sub>3</sub>
Glass slide	11.8	4.43	1.58	72.9	<0.05	0.72	8.12	<0.05	<0.10
Soda-lime glass (Na-Ca-Si)	12.3	1.78	3.78	67.8	<0.05	3.80	9.20	<0.05	<0.10
Potash-lime glass (K-Ca-Si)	<0.10	1.79	2.97	52.5	1.75	20.7	19.9	<0.05	<0.10
Mixed-alkali glass (K-Na-Ca-Si)	9.49	3.89	3.29	62.1	0.14	6.88	13.4	0.37	0.40

Despite the increasing amounts of lead added, it was impossible to see a significant change in the chemical composition of the different base glasses. The glass with a 1:4 proportion between SiO<sub>2</sub> and PbO experienced a high lead loss due to lead volatilization, shifting the proportion of SiO<sub>2</sub>:PbO to (1:2.5). In the binary SiO<sub>2</sub>-PbO systems, a sharper deflection of PbO volatilization occurs with the increase in lead content, mainly above 80 wt% PbO [7,24]. It is also possible to see small amounts of aluminum contamination through the different glasses and sodium, potassium, and iron in the SiO<sub>2</sub>:PbO (1:4) glass. All these elements can appear due to contamination from the crucible during the melting process. The increasing amount of these elements in the SiO<sub>2</sub>:PbO (1:4) glass can be related to the higher amount of lead in the initial formulation, which leads to a higher contact time of the molten glass with the crucible walls as the glass reaches the melting point faster and at a lower temperature. As these contaminations represent less than 3 wt% of the base glasses composition, they would not influence the future results of this study.

The composition of the different substrate glasses is shown in Table 3. These glasses represent typical compositions from historical stained-glass windows: soda-lime silicate glass, potash-lime silicate glass, and mixed-alkali glass [17]. The glass slide is also classified as soda-lime silicate glass.

The X-ray diffraction results showing the crystallographic phases of the coloring agents and other materials tested are represented in Table 4. All the diffractograms can be consulted in Appendix B, Figures A1–A11. For the burned iron, it was only possible to identify it in one state of oxidation after the burning, iron (III) oxide (hematite ( $\text{Fe}_2\text{O}_3$ )). On the other hand, the burned copper is composed of a mixture of copper oxides in two different oxidation states, copper (I) oxide (cuprite ( $\text{Cu}_2\text{O}$ )) and copper (II) oxide (tenorite ( $\text{CuO}$ )). For the mixture of burned tin and lead, independent oxides of lead (massicot ( $\text{PbO}$ )) and minium ( $\text{Pb}_3\text{O}_4$ )) and tin (cassiterite ( $\text{SnO}_2$ )) were formed instead of a mixed compound as a lead stannate ( $\text{Pb}_2\text{SnO}_4$ ). It was also possible to confirm the crystallography of the chosen practical grade (PA) compounds: burned lead ( $\text{PbO}$ ), manganese ( $\text{MnO}_2$ ), hematite ( $\text{Fe}_3\text{O}_4$ ), alumina ( $\text{Al}_2\text{O}_3$ ), and antimony ( $\text{Sb}_2\text{O}_3$ )). Iron (III) oxide (hematite ( $\text{Fe}_2\text{O}_3$ )) was also identified for the pigments/earths of natural hematite and burned umber. This was unexpected, as usually, these natural pigments have a significant number of impurities, such as aluminum oxide in the hematite and manganese in the burned umber [18]. Hydrocerussite ( $(\text{Pb}_3(\text{CO}_3)_2(\text{OH})_2)$ ), which is a hydrated form of cerussite ( $\text{PbCO}_3$ ), was identified in the lead white pigment [18].

**Table 4.** Crystallographic phases of the coloring agents and other materials obtained by XRD.

Crystallographic Phases	
Burned iron	Hematite ( $\text{Fe}_2\text{O}_3$ )
Burned copper	Cuprite ( $\text{Cu}_2\text{O}$ ), Tenorite ( $\text{CuO}$ )
Manganese PA	Pyrolusite ( $\text{MnO}_2$ )
Hematite PA	Hematite ( $\text{Fe}_2\text{O}_3$ )
Natural hematite	Hematite ( $\text{Fe}_2\text{O}_3$ ), Quartz ( $\text{SiO}_2$ )
Burned umber	Hematite ( $\text{Fe}_2\text{O}_3$ )
Alumina PA	Corundum ( $\text{Al}_2\text{O}_3$ )
Antimony PA	Senarmontite ( $\text{Sb}_2\text{O}_3$ )
Burned SnPb	Cassiterite ( $\text{SnO}_2$ ), Massicot ( $\text{PbO}$ ), Minium ( $\text{Pb}_3\text{O}_4$ )
Burned lead ( $\text{PbO}$ PA)	Massicot ( $\text{PbO}$ )
Lead white	Hydrocerussite ( $\text{Pb}_3(\text{CO}_3)_2(\text{OH})_2$ )

### 3.2. Grisaille Properties

#### 3.2.1. Crystallographic Characterization

Table 5 shows the crystalline phases of the model grisaille, which, as described in Table 1, was produced with a mixture of burned iron and copper. The results showed the presence of hematite ( $\text{Fe}_2\text{O}_3$ ), cuprite ( $\text{Cu}_2\text{O}$ ), and tenorite ( $\text{CuO}$ ). These three compounds were previously identified in the raw material characterization (Table 4). However, the tenorite ( $\text{CuO}$ ) has a much higher intensity in the model grisaille (Figure A12) than in the burned copper diffraction result (Figure A2). This indicates that some cuprite oxidizes into tenorite during the grisaille's firing. At these firing conditions, tenorite is also a more stable compound [25].

The results for the grisailles (Figures A13–A17) where different coloring agents were used and the other materials added are also shown in Table 5. The identified components were the same as the ones identified in the raw materials (Table 4), except for the burned lead and lead white that formed the compound called iron barysilite ( $\text{Pb}_8\text{Fe}(\text{Si}_2\text{O}_7)_3$ ) after the firing process of the grisailles.

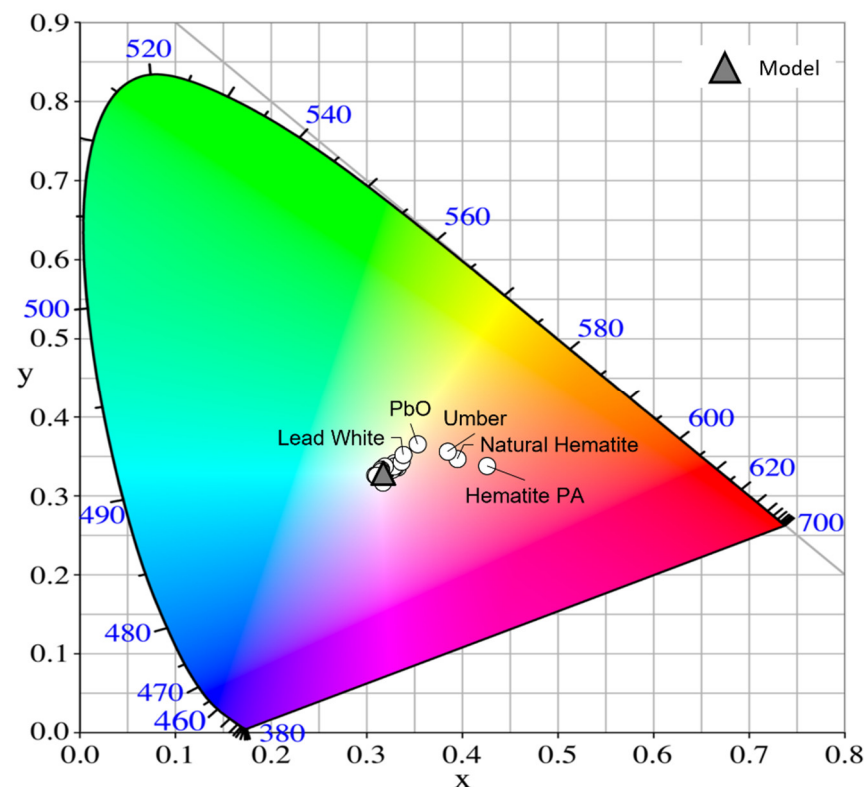
The crystalline phases identified correspond to previously identified components in historical grisaille samples characterized and found in the literature [11,12,26–28].

**Table 5.** Crystallographic phases of selected grisaille samples obtained by XRD.

Grisailles	Crystallographic Phases
Model	Hematite ( $\text{Fe}_2\text{O}_3$ ); Cuprite ( $\text{Cu}_2\text{O}$ ); Tenorite ( $\text{CuO}$ )
Hematite PA	Hematite ( $\text{Fe}_2\text{O}_3$ )
Natural hematite	Hematite ( $\text{Fe}_2\text{O}_3$ ); Quartz ( $\text{SiO}_2$ )
Burned umber	Hematite ( $\text{Fe}_2\text{O}_3$ )
Burned lead	Hematite ( $\text{Fe}_2\text{O}_3$ ); Cuprite ( $\text{Cu}_2\text{O}$ ); Tenorite ( $\text{CuO}$ ); Iron barysilite ( $\text{Pb}_8\text{Fe}(\text{Si}_2\text{O}_7)_3$ )
Lead white	Hematite ( $\text{Fe}_2\text{O}_3$ ); Cuprite ( $\text{Cu}_2\text{O}$ ); Tenorite ( $\text{CuO}$ ); Iron barysilite ( $\text{Pb}_8\text{Fe}(\text{Si}_2\text{O}_7)_3$ )

### 3.2.2. Colorimetry

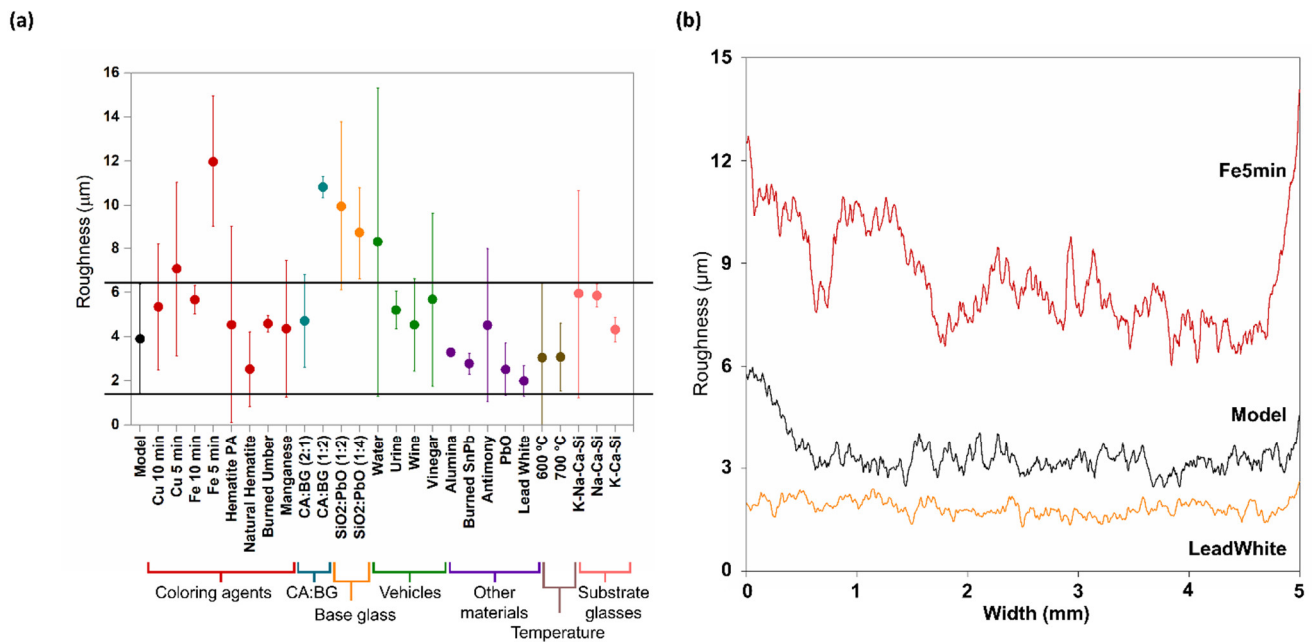
The results from the colorimetric study are represented in Figure 2. It is possible to observe that the results for almost all the samples agree with the model grisaille, where similar color was observed. The use of hematite (PA or natural) and burned umber changes the color toward a warmer hue (red). These color alterations are directly related to the original colors of raw materials, as the hematite and burned umber are red-brownish pigments [18,29]. In addition, after the firing process, it was not possible to see any changes in the crystalline compounds used for these grisailles, as visible in Table 5 results, where hematite ( $\text{Fe}_2\text{O}_3$ ) was identified as the main compound for these three grisailles.

**Figure 2.** Colorimetric xy diagram for the produced samples.

Additives can also influence the final color of the grisaille. The lead white and the PbO turn the grisailles toward a yellowish color, as shown in Figure 2. This change can occur because when these two lead compounds are added to the grisaille mixture, a new compound called iron barysilite ( $\text{Pb}_8\text{Fe}(\text{Si}_2\text{O}_7)_3$ ) is formed (Table 5). This compound is a lead-rich iron silicate that can be a low-temperature precursor of the melanotekite ( $\text{Pb}_2\text{Fe}_2(\text{Si}_2\text{O}_7)\text{O}_2$ ) with a yellowish/greenish hue, which can influence the final color of the grisaille [11,30,31].

### 3.2.3. Roughness

The results from the roughness analyses are represented in Figure 3.



**Figure 3.** Results from the roughness analysis, (a) graphical representation from the average roughness ( $Ra^*$ ) and their standard deviations of the produced grisaille samples, (b) graphical representation of the roughness variation throughout the sample length.

The interpretation of these results must consider that despite the painting technique for applying the paint layers into the substrate glass was the same, and it was made by hand, so the final grisaille layers are susceptible to handcraft-related variations.

Considering what was described before, it is possible to see that the average roughness of the different grisaille samples does not present a significant variation from the model grisaille ( $1.99 \pm 0.28 < Ra^* < 11.96 \pm 1.20 \mu\text{m}$ ), being the average of almost all the samples inside the range of the model grisaille standard deviation, as shown in Figure 3a. Nevertheless, the samples where the copper and iron were only grounded for 5 min presented a higher rugosity ( $7.08 \pm 1.59 \mu\text{m}$  and  $11.96 \pm 1.20 \mu\text{m}$ , respectively) because the size of the metal's oxides was larger (Figure 3a). Nonetheless, iron presents a higher rugosity than copper because iron has higher hardness [20] in comparison and, therefore, needs more grinding time to obtain a thinner powder.

In the grisaille, with more base glass (CA:BG (1:2)), the roughness almost doubles the value ( $10.81 \pm 0.20 \mu\text{m}$ ) compared with the model sample and with the one with less base glass (CA:BG (2:1)) ( $4.71 \pm 0.85 \mu\text{m}$ ). This can indicate that the time or temperature used during the firing was insufficient to soften this higher quantity of base glass and even out and flatten the painted layer.

The different base glasses used (SiO<sub>2</sub>:PbO (1:2) and SiO<sub>2</sub>:PbO (1:4)) also give higher rugosity ( $9.95 \pm 1.54 \mu\text{m}$  and  $8.71 \pm 0.84 \mu\text{m}$ , respectively) to the grisaille when compared with the one used for the model grisaille (SiO<sub>2</sub>:PbO (1:3)) ( $3.90 \pm 0.99 \mu\text{m}$ ). These glasses are the ones that have less lead in their composition, as shown in Table 2. Therefore, they have a slightly higher melting temperature being less flattened.

An increase in rugosity ( $8.30 \pm 2.82 \mu\text{m}$ ) and its range of standard deviation was also observed when water without any binding agent was used as a vehicle (Figure 3a). This is a consequence of the difficult manipulation and application of the paint only using water as a vehicle. Less plastic paint is obtained during the application, which leads to a struggle to achieve a final smooth and even layer.

The standard deviation of the results also gives information about the samples because smaller ranges, such as the samples with burned umber, alumina, and burned tin and lead, can indicate a homogeneous surface throughout the sample.

Higher rugosities can increase the grisailles porosity, which, combined with bubbles and fissures, can increase the susceptibility of water penetration through the paint layers, accelerating the degradation process [11–13,16,32–35]. This is visible in the samples from the Czech Republic, studied by Čílová et al., where it was possible to visualize vertical and horizontal cracks throughout the paint layer [35]. These cracks probably facilitated the water penetration and were responsible for the high corrosion observed in the substrate glasses under the grisaille layers, ultimately leading to the paint layers' pulverization.

Figure 3b shows the roughness variation throughout the length of the samples, representing the samples with the higher (Fe 5 min sample) and lowest (lead white sample) rugosity measured, as well as the model sample result. It is possible to observe that the grisaille with a higher rugosity (Fe 5 min) also presents higher variation throughout the length of the sample with its uneven line, and the grisaille with the lowest rugosity (lead white) presents a more even line throughout the length of the sample.

#### 3.2.4. Contact Angle

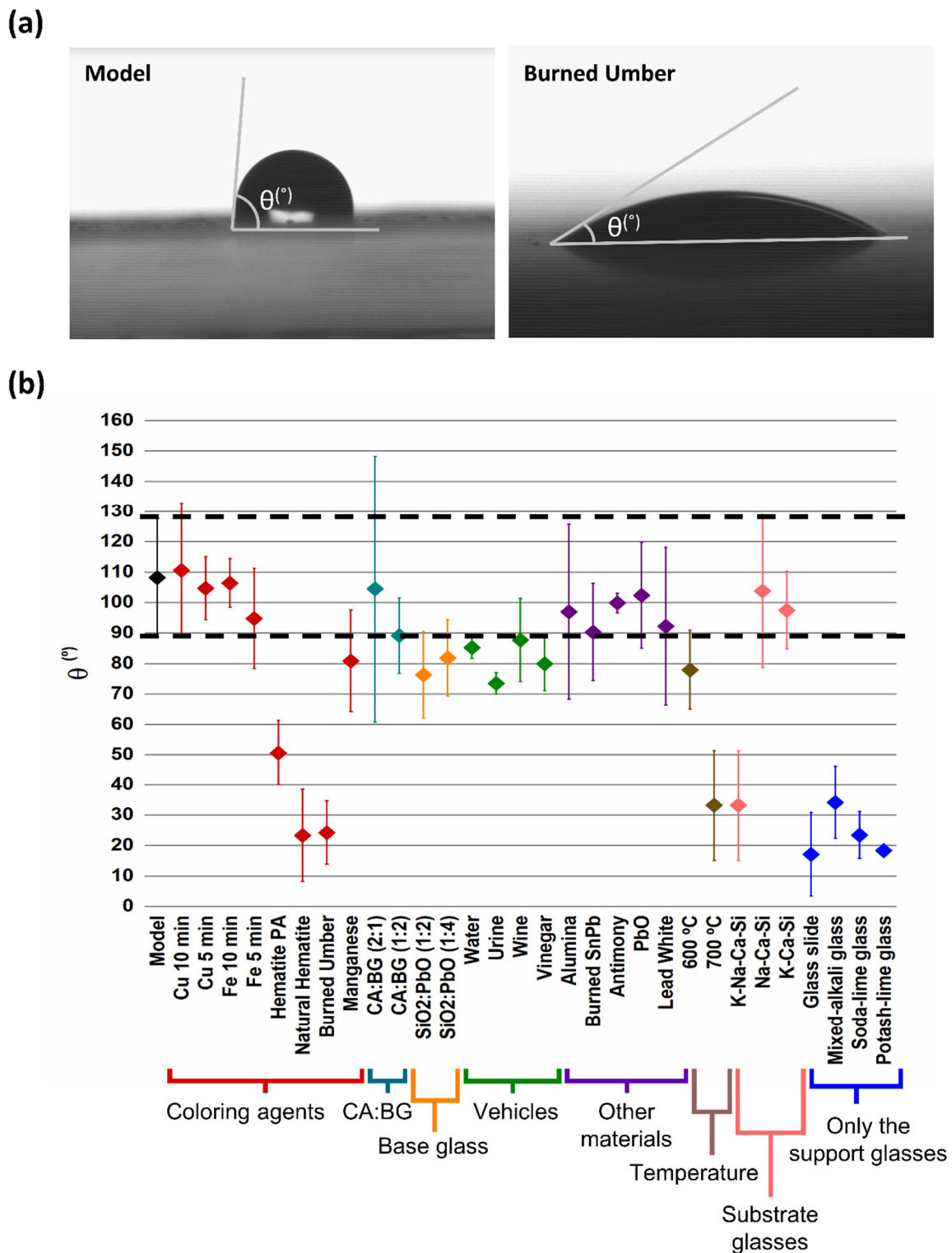
Figure 4 represents the results of the contact angle measurement. The higher the contact angle, the more hydrophobic the sample is. In Figure 4a, it is possible to visually compare the water drops' behavior when in contact with the model sample and with a less hydrophobic one (burned umber).

The results showed a general decrease in the contact angle value when comparing the samples with the model grisaille (Figure 4b), which is related to a decrease in the hydrophobic characteristics of the samples, demonstrating the impact that the different variables can have in the grisailles water affinity.

The samples that showed a higher affinity with water were the ones where hematite (PA or Natural) and burned umber were used, as well as the grisaille fired at 700 °C and the one painted on a mixed-alkali glass (Figure 4b).

These results do not match the roughness results (Figure 3). It is expected that the samples with higher rugosity were the more hydrophilic ones. However, the water fixation and penetration in the grisaille paint layers depend on several factors. For example, unsuitable firing temperatures and incompatibilities between the grisaille and glass support can create bubbles and tensions, which can lead to the formation of fissures helping the water penetration [16,35,36]. This is visible in grisailles from the windows of the church of S. Giovanni and Paolo in Venice (Italy) [16], which showed fissures in the grisaille layers parallel to the glass support, which were caused by a wrong firing temperature. This can justify the lower contact angles presented by the grisaille fired at 700 °C and the one painted on a mixed-alkali glass. The intrinsic properties of some raw materials can also influence the hydrophilic characteristic of the painted layers. This can be observed in the grisailles where hematite (PA and Natural) and burned umber were used, which also presented lower angles. Shrimali et al. previously studied hematite ores used to have contact angles between 60 and 10 degrees [37] depending on the surface hydroxylation, which agrees with the results presented in Figure 4b. The burned iron did not present similar results despite also being hematite. This could happen because it was produced by burning steel pieces, which creates a more aggregated and less thin powder with a less exposed contact surface.

The contact angles from the different support glasses without grisaille paint were also measured, and the results are shown in Figure 4b. Comparing the results from the support glasses with the ones obtained for the grisailles painted on them, it is possible to understand that most support glasses present lower contact angles, being more hydrophilic than the grisaille layers. This indicates that the grisaille layer, in its majority, can become a protective layer, diminishing the water affinity of the surface. However, this also depends on the raw materials' intrinsic characteristics, the firing temperature, the compatibility between the grisaille and the substrate glasses, and the presence of fissures or bubbles.



**Figure 4.** Contact angle results (a) examples of pictures taken during the test and (b) graphical representation of contact angle for all the samples (model sample in black).

### 3.3. Adherence Tests

The adherence tests were made to analyze the compatibility between the grisailles and substrate glasses, shown in Table 6. The model sample was classified as 1, where only the superficial layer was cut, as it is practically impossible to observe the marks in the painted sample, but with residual detachment visualized in the adhesive tape (Table 6). Eighteen of

the samples (Fe 10 min, Fe 5 min, Cu 10 min, Cu 5 min, BG (SiO<sub>2</sub> + PbO 1:2), BG (SiO<sub>2</sub> + PbO 1:4), water, urine, wine, vinegar, alumina, antimony, burned PbSn, 700 °C, CA:BG (1:2), mixed-alkali glass, soda-lime glass, and potash-lime glass) were also classified as 1 showing similar results as the one for the model grisaille. Indicating that these variables will not significantly impact the adhesion of the grisaille paint layers. Some of these variables' results are shown in Table 6.

**Table 6.** Results from the adhesion test.





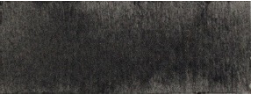

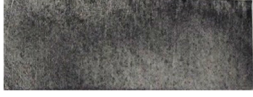

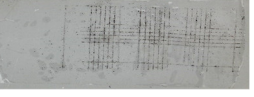
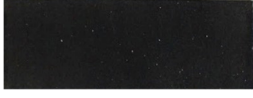

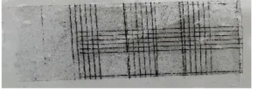


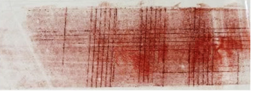



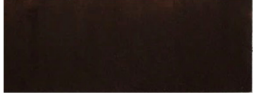


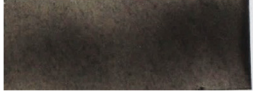
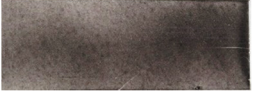

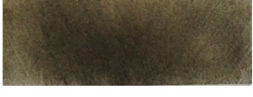
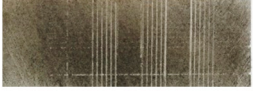

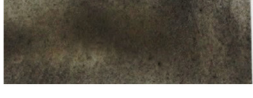

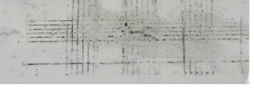

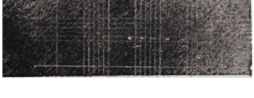
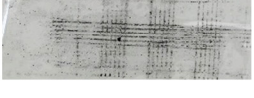
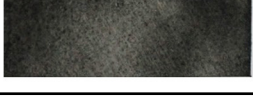
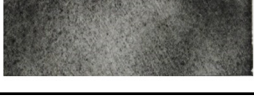







Variable	Painted Samples		Adhesion Test	
	(Before Adhesion Tests)	(Reflected Light)	Adhesive Tape	Classification
Model grisaille				1
Fe 5 min				1
Cu 5 min				1
Manganese				3
Hematite PA				4
Natural hematite				3
Burned umber				4
Burned SnPb				1
PbO				2
Lead white				2
600 °C				2
700 °C				1

Table 6. Cont.

Variable	Painted Samples		Adhesion Test	
	(Before Adhesion Tests)	(Reflected Light)	Adhesive Tape	Classification
CA:BG (2:1)				2
CA:BG (1:2)				1

The samples where pigments were used as coloring agents were the ones that showed less adhesion of the grisaille (Table 6). The samples with manganese and natural hematite had an intense detachment, classified as 3, and the hematite PA and burned umber grisailles were classified as 4 (Table 6). In general, the pigments have smaller particle sizes than the burned metals leading to an increase in the contact surface between the coloring agents and the base glass, needing more base glass to obtain a suitable fixation of the coloring agents. The proportion between the base glass and coloring agents must be enough to cover the metal oxide grains to guarantee suitable adhesion to the substrate, as described by Bettembourg [32]. These results also agree with the contact angle results (Figure 4) where hematite (PA and natural) and burned umber were added and also showed a higher affinity with water, reinforcing that the addition of these raw materials seems to create less resistant grisailles.

The grisailles where burned lead and lead white were used also showed poor adhesion and were classified as 3 (Table 6). These compounds can also create unbalanced grisailles, altering the ratios between coloring agents and base glasses.

A lower temperature (600 °C) can also be insufficient to create a suitable adhesion, being probable that the softening temperature was not reached, as well as a higher proportion of coloring agent to base glass.

Table 7 shows some examples of the cleaning test. The results showed that the model grisaille is not susceptible to solvents, with only some fibers of the cotton swab being visible on the surface, and the cotton swabs did not present any grisaille trace (Table 7). Similar results were observed in 18 of the samples (Fe 10 min, Fe 5 min, Cu 10 min, Cu 5 min, BG (SiO<sub>2</sub> + PbO 1:2), BG (SiO<sub>2</sub> + PbO 1:4), water, urine, wine, vinegar, alumina, antimony, burned PbSn, 700 °C, CA:BG (1:2), mixed-alkali glass, soda-lime glass, and potash-lime glass) the same stable samples as in the adhesion tests.

The grisailles that showed a higher susceptibility to the solvents are the ones where burned umber, burned lead, and lead white were used, with the total removal of the painted layers. The grisailles where manganese and hematite were used showed traces of the grisaille on the cotton swabs but without removal marks on the painted layers (Table 7). These results show that a superficial layer was susceptible to the solvents, but the underneath layer was more resistant to cleaning. The solvents that have a higher impact are ethanol and acetone.

The cleaning test also proved that a temperature of 600 °C is insufficient to create a cohesive and well-adhered grisaille. The solvents can remove the painted layer, and the ones based on ethanol seem more aggressive, leaving intense marks on the surface (Table 7). The sample with a higher proportion of coloring agent can also interfere with the grisaille adhesion, showing some traces of paint on the ethanol cotton swab (Table 7).

The cleaning and adhesion tests (Table 6) agree with each other, as the less adhered grisailles are more susceptible to the solvents tested.



Table 7. Results from the cleaning test.

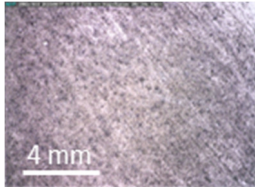
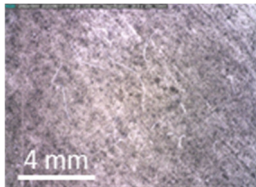
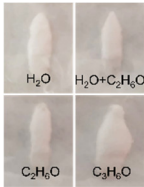





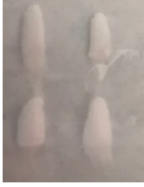
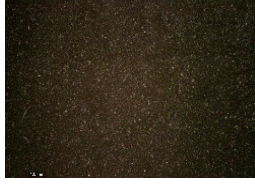
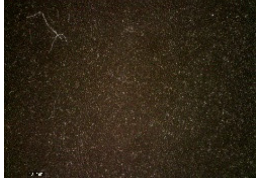

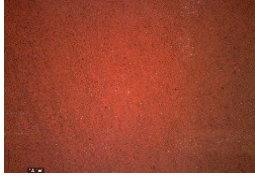
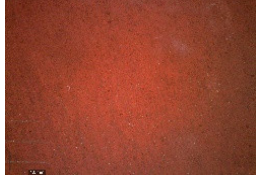







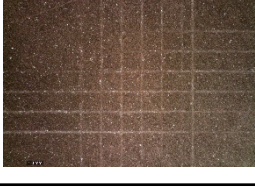
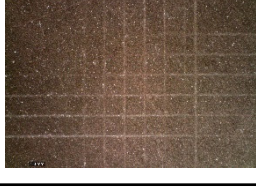



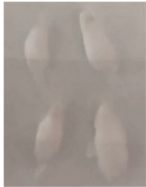


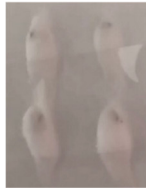


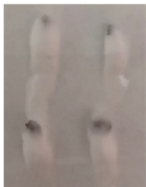


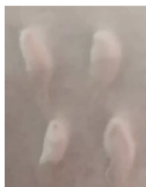





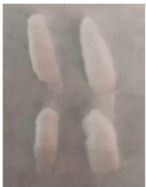
Variable	Before	After	Swabs
Model			 $H_2O$ $H_2O+C_2H_6O$ $C_2H_6O$ $C_3H_8O$
Fe 5 min			
Cu 5 min			
Manganese			
Hematite PA			
Natural hematite			
Burned Umber			
Burned SnPb			

Table 7. Cont.

Variable	Before	After	Swabs
PbO			
Lead White			
600 °C			
700 °C			
CA:BG (2:1)			
CA:BG (1:2)			

#### 4. Conclusions

This work has demonstrated that raw materials directly affect the properties and appearance of grisailles.

Iron and copper produce similar hues; however, pigments, such as hematite (PA or natural) and burned umber, and other materials, such as lead oxide or lead white, can give specific characteristics or appearances to the final paints.

The raw materials also affect the affinity to water. Less hydrophobic materials, such as hematite and burned umber, showed an increase in the hydrophilic properties of the samples. A significant impact was also visible at temperatures of 700 °C and when a less compatible substrate glass (mixed-alkali glass) was used. These reinforce the idea that the water absorbance and penetration depend not only on the rugosity, as these results do not agree with the roughness analysis.

Considering the analysis, the average roughness ( $Ra^*$ ) did not show significant changes in the majority of cases. Concluding that the most important factor is the size of the coloring agents, and it is essential to adapt the grinding time to the hardness of each raw material in the grisailles production.

Another factor that can significantly impact the long-term stability of the grisailles is the unbalanced volume between base glass and coloring agent particles. The adhesion and cleaning test results proved this. As in both cases, the grisailles with hematite (PA or natural), burned umber, and manganese showed less resistance to the cutting blades and solvents, justified by the small particle size of these pigments, which created unbalanced grisailles in volume. Additionally, the grisailles with hematite (PA and natural) appeared to have a superficial layer susceptible to the solvents and another one that was more cohesive and resistant underneath.

With the characterization and tests carried out in this study, it was possible to understand that the grisaille stability can be affected by different reasons. The variables chosen to be tested allowed for establishing the main factors that must be considered while choosing the raw materials to produce grisaille. The coloring agents used and their treatments before being added to the grisailles can greatly affect the final paint layer, not only in its color but also in its rugosity, affinity with water, and adhesion and chemical resistance. The different base glasses mainly affected the grisailles rugosity, as their lead content will influence the firing conditions needed. The different vehicles tested did not greatly impact the final grisailles. It was only possible to observe the rugosity affected by the use of water due to the difficult manipulation of the grisaille and its application before firing. Paired with the coloring agents, the other materials can also significantly affect the grisailles, mainly the burned lead and lead white. Not only was it verified that they would impact the color and the grisailles adhesion and chemical resistance, but also that during the firing process, they will decompose and link themselves with components from the coloring agents and base glass, forming new mixed compounds. The temperature is another variable to consider as unsuitable firing conditions affected the grisailles, demonstrated by the contact angle measurements and the results of the adhesion and cleaning tests. As described in the literature and verified in this study, the proportions between the different grisaille components can also be a key factor in the grisailles stability. The tests verified that unbalanced proportions could affect the grisailles rugosity, mainly their physical and chemical adhesion to the glass support. The different substrate glasses tested showed suitable compatibility with the grisailles. Nevertheless, it is always a factor to take into consideration.

Furthermore, aging tests on the produced samples will significantly contribute to understanding the long-term stability and possible corrosion mechanisms of these grisailles, as well as to verify the real impact that each of the variables tested in this study will have on the grisaille layers degradation.

**Author Contributions:** Conceptualization, M.V. and T.P.; methodology, C.M.; validation, T.P.; investigation, C.M. and J.V.P.; writing—original draft preparation, C.M.; writing—review and editing, C.M., M.V., J.V.P. and T.P.; supervision, M.V. and T.P. All authors have read and agreed to the published version of the manuscript.

**Funding:** This research was funded by Fundação para a Ciência e Tecnologia de Portugal (projects UIDB/00729/2020, UIDP/00729/2020, UIDB/50025/2020-2023, researcher grant CEECIND/02249/2021 and doctoral grant ref. PD/BD/136673/2018).

**Institutional Review Board Statement:** Not applicable.

**Informed Consent Statement:** Not applicable.

**Data Availability Statement:** Not applicable.

**Acknowledgments:** The authors wish to thank María José Velasco (ICV-CSIC, Spain) for the XRF analysis, Daniela Hernandez (ICV-CSIC, Spain) for her help during the contact angle analysis, and Mónica Álvarez de Burgo (IGEO-CSIC-UCM, Spain) for the access to the colorimetric and roughness analysis equipment.

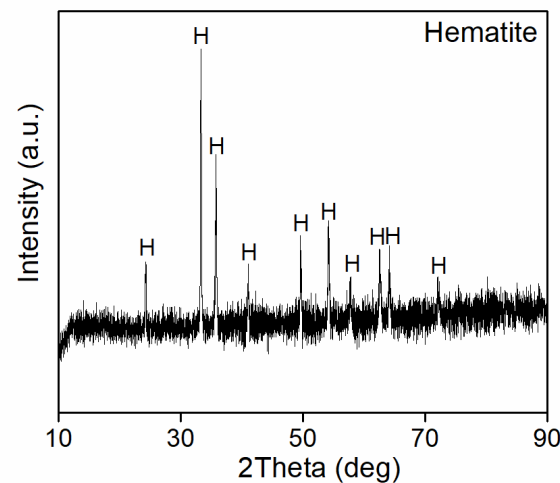
**Conflicts of Interest:** The authors declare no conflict of interest.

## Appendix A

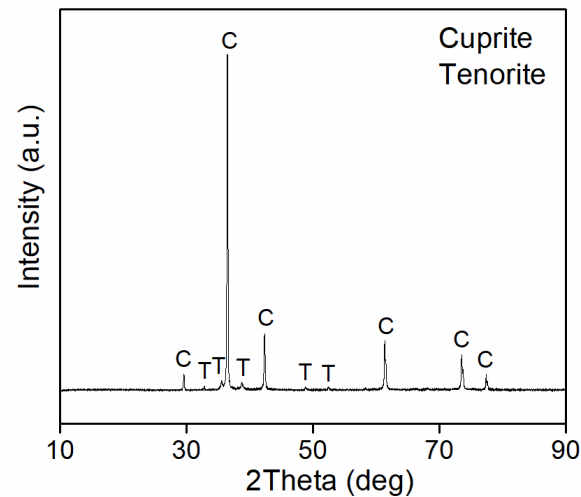
**Table A1.** Brands/manufacturers of the commercial materials used in the samples production.

Compound	Brand/Manufacturer
SiO <sub>2</sub>	Sigma-Aldrich Chemistry
PbO	Sigma-Aldrich Chemistry0
SnO <sub>2</sub>	Alfa Aesar Chemicals
Fe <sub>2</sub> O <sub>3</sub>	Riedel-de Haën–Honeywell Research Chemicals
MnO <sub>2</sub>	Panreac Química SLU–ITW Reagents
Al <sub>2</sub> O <sub>3</sub>	Fluka–Honeywell Research Chemicals
Sb <sub>2</sub> O <sub>3</sub>	Alfa Aesar Chemicals
Burned Umber	Winsor and Newton
Gum Arabic	Debitus–Peintures pour verre

## Appendix B



**Figure A1.** XRD result for burned iron. Hematite (H) was identified.



**Figure A2.** XRD result for burned copper. Cuprite (C) and tenorite (T) were identified.

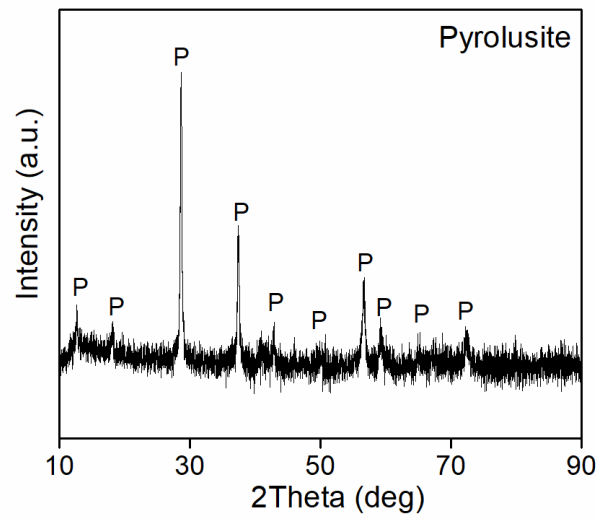


Figure A3. XRD result for manganese PA. Pyrolusite (P) was identified.

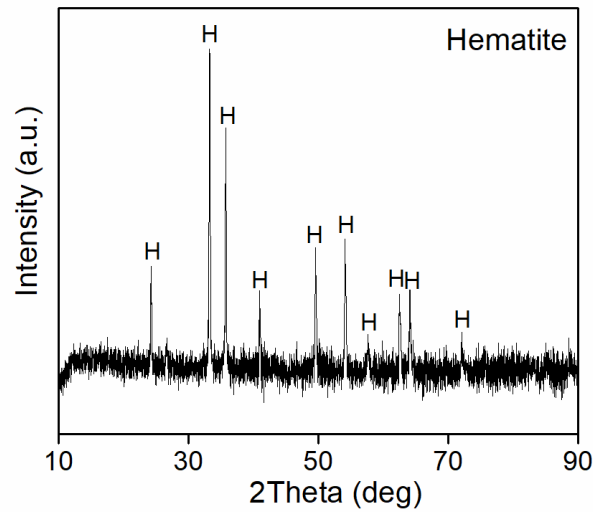


Figure A4. XRD result for hematite PA. Hematite (H) was identified.

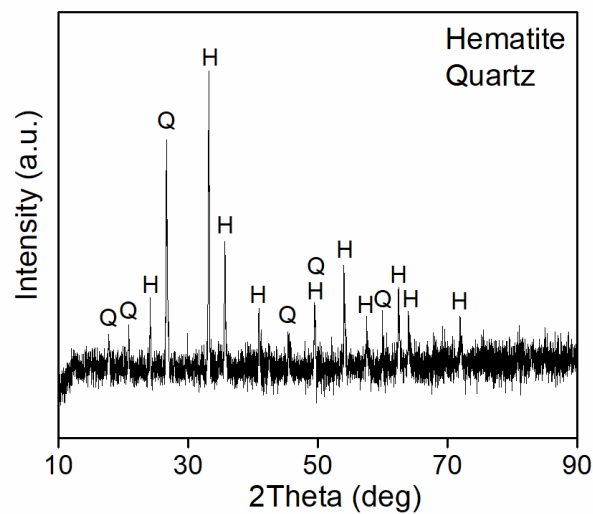


Figure A5. XRD result for natural hematite. Hematite (H) and quartz (Q) were identified.

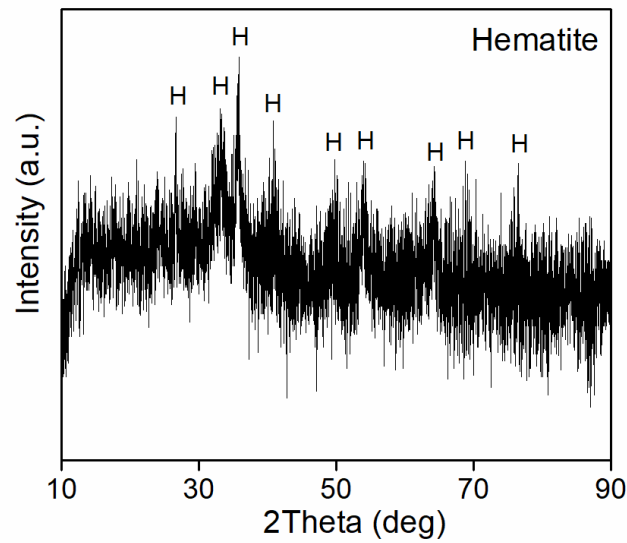


Figure A6. XRD result for burned umber. Hematite (H) was identified.

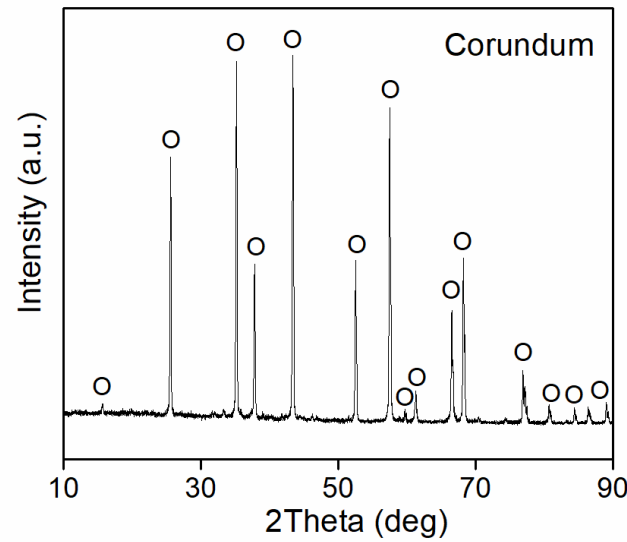


Figure A7. XRD result for alumina PA. Corundum (O) was identified.

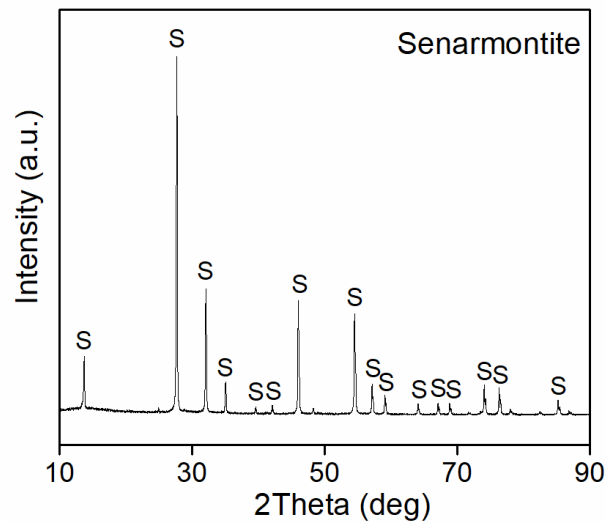
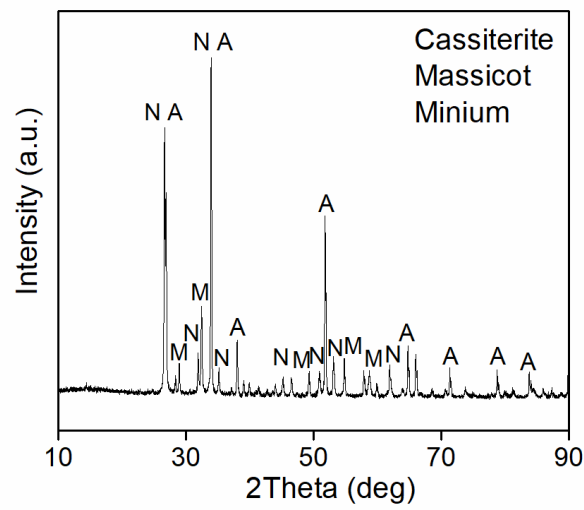
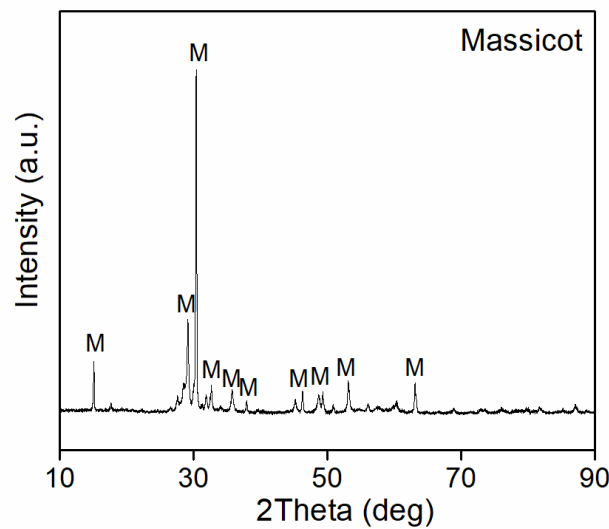


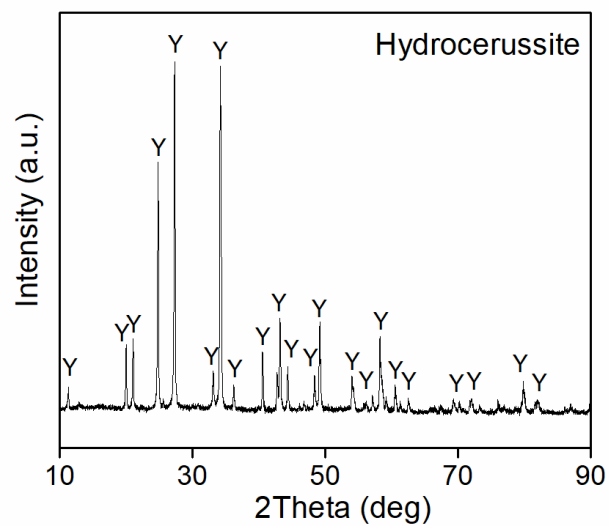
Figure A8. XRD result for antimony PA. Senarmonite (S) was identified.



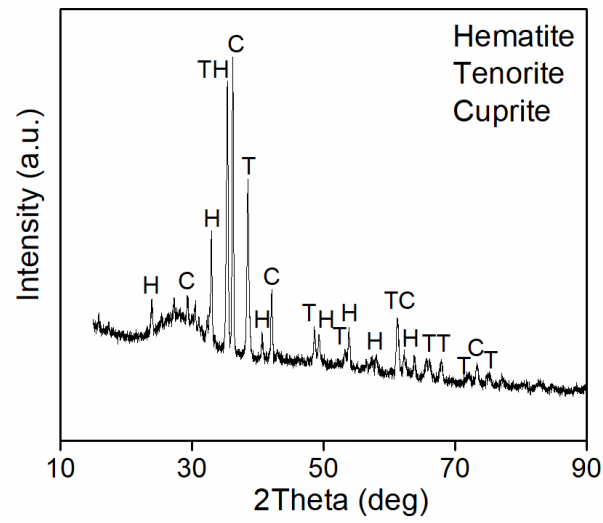
**Figure A9.** XRD result for burned tin and lead. Cassiterite (A), massicot (M), and minium (N) were identified.



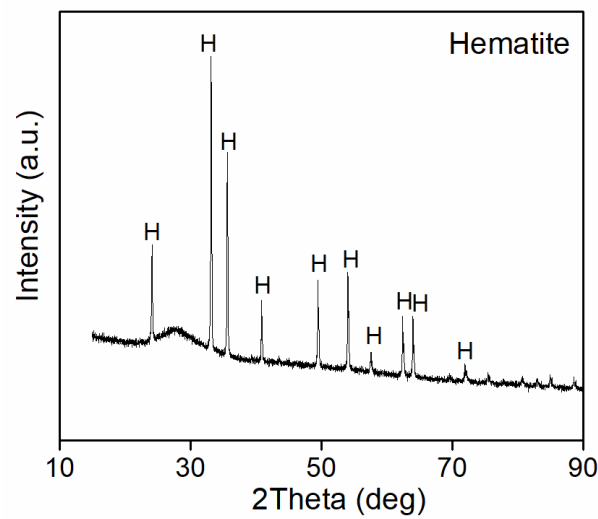
**Figure A10.** XRD result for burned lead. Massicot (M) was identified.



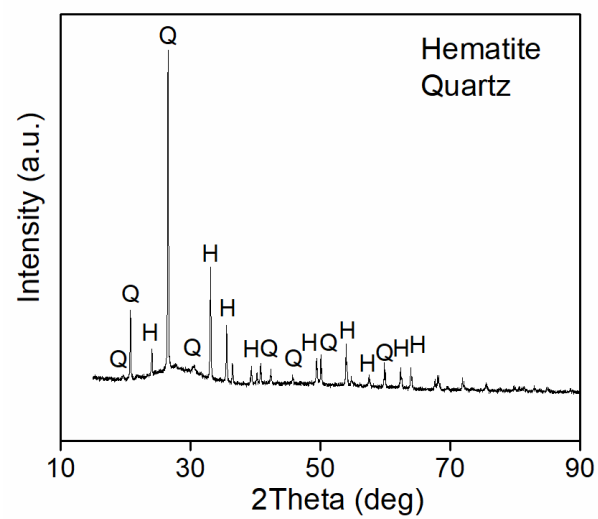
**Figure A11.** XRD result for lead white. Hydrocerussite (Y) was identified.



**Figure A12.** XRD result from the model grisaille. Hematite (H), tenorite (T), and cuprite (C) were identified.

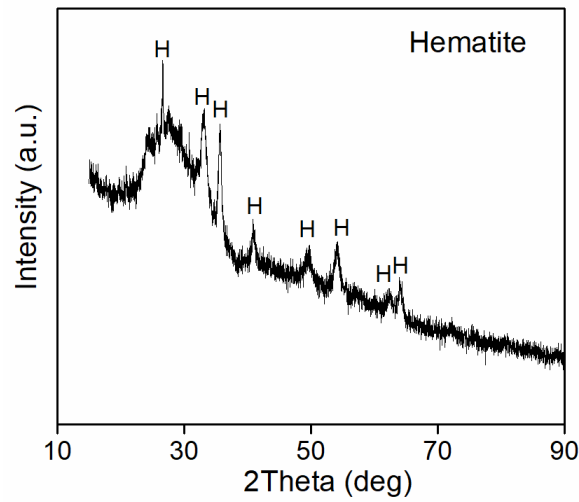


**Figure A13.** XRD result from the grisaille where hematite PA was used. Hematite (H) was identified.

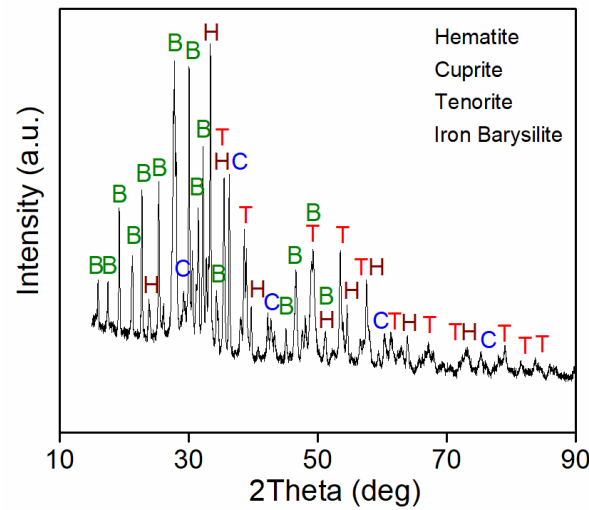


**Figure A14.** XRD result from the grisaille where natural hematite was used. Hematite (H) and quartz (Q) were identified.

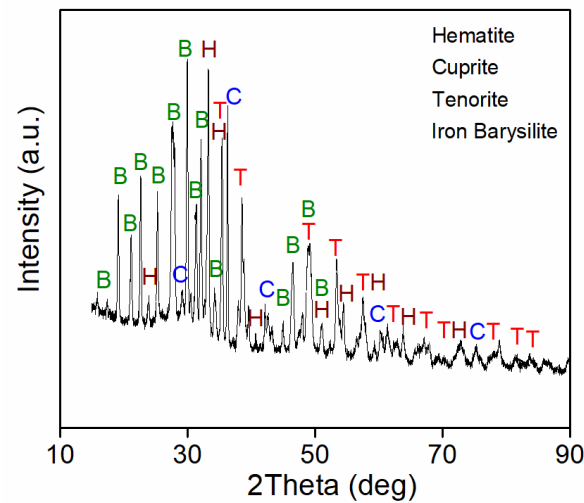




**Figure A15.** XRD result from the grisaille where burned umber was used. Hematite (H) was identified.



**Figure A16.** XRD result from the grisaille where burned lead was used. Hematite (H), cuprite (C), tenorite (T), and iron barysilite (B) were identified.



**Figure A17.** XRD result from the grisaille where lead white was used. Hematite (H), cuprite (C), tenorite (T), and iron barysilite (B) were identified.

## References

1. Schalm, O. *Characterization of Paint Layers in Stained-Glass Windows: Main Causes of the Degradation of Nineteenth Century Grisaille Paint Layers*; Universiteit Antwerpen: Antwerpen, Belgium, 2000.
2. Machado, C.; Machado, A.; Palomar, T.; Vilarigues, M. Grisaille in Historical Written Sources. *J. Glass Stud.* **2019**, *61*, 71–86.
3. Vilarigues, M.; Machado, C.; Machado, A.; Costa, M.; Alves, L.C.; Cardoso, I.P.; Ruivo, A. Grisailles: Reconstruction and Characterization of Historical Recipes. *Int. J. Appl. Glas. Sci.* **2020**, *11*, 756–773. [[CrossRef](#)]
4. Machado, C.; Vilarigues, M.; Palomar, T. Historical Grisailles Characterisation: A Literature Review. *J. Cult. Herit.* **2021**, *49*, 239–249. [[CrossRef](#)]
5. Merrifield, M. *Original Treatises on the Arts of Paintings*; Dover Publications: Mineola, NY, USA, 1849; Volume 1.
6. Bontemps, G. *Guide du Verrier: Traité Historique et Pratique de la Fabrication des Verres, Cristaux, Vitraux*; Librairie du Dictionnaire des Arts et Manufactures: Paris, France, 1868.
7. Volf, M.B. *Chemical Approach to Glass*, 2nd ed.; Elsevier: Amsterdam, The Netherlands, 1984.
8. Foster, J. *Lives of the Most Eminent Painters, Sculptors, and Architects: Translated from the Italian of Giorgio Vasari*; Bohn, H.G., Ed.; Modern Library: New York, NY, USA, 1855.
9. Verità, M. Paintwork in Medieval Stained-Glass Windows: Composition, Weathering, and Conservation. In *Proceedings of the Forum for the Conservation and Restoration of Stained Glass, the Art of Collaboration: Stained-Glass Conservation in the Twenty-First Century, New York City, NY, USA, 1–3 June 2009*; Shepard, M.B., Pilosi, L., Stroble, S., Eds.; Harvey Miller: London, UK, 2010; pp. 210–216.
10. Rodrigues, A.; Coutinho, M.L.; Machado, C.; Alves, L.C.; Machado, A.; Vilarigues, M. An Overview of Germanic Grisailles through the Stained-Glass Collection at Pena Palace. *Heritage* **2022**, *5*, 1003–1023. [[CrossRef](#)]
11. Pradell, T.; Molina, G.; Murcia, S.; Ibáñez, R.; Liu, C.; Molera, J.; Shortland, A. Materials, Techniques and Conservation of Historic Stained Glass “Grisailles”. *Int. J. Appl. Glass Sci.* **2016**, *7*, 41–58. [[CrossRef](#)]
12. Verità, M.; Nicola, C.; Sommariva, G. The Stained Glass Windows of the Sainte Chapelle in Paris: Investigations on the Origin of the Loss of the Painted Work. *AIHV Ann. 16 Congrès* **2003**, 347–351.
13. Vilarigues, M.; Da Silva, R.C. Ion Beam and Infrared Analysis of Medieval Stained Glass. *Appl. Phys. A Mater. Sci. Process.* **2004**, *79*, 373–378. [[CrossRef](#)]
14. Schalm, O.; Janssens, K.; Caen, J. Characterization of the Main Causes of Deterioration of Grisaille Paint Layers in 19th Century Stained-Glass Windows by J.-B. Capronnier. *Spectrochim. Acta Part B At. Spectrosc.* **2003**, *58*, 589–607. [[CrossRef](#)]
15. Bettembourg, J.-M. Altération et Problèmes de Conservation Des Grisailles. *Corpus Vit. News Lett.* **1984**, *37/38*, 5–7.
16. Verità, M. Composition, Structure et Mécanisme de Détérioration Des Grisailles. *Doss. Comm. R. Monum. Sites Fouill.* **1996**, *3*, 61–68.
17. Palomar, T.; Redol, P.; Almeida, I.C.; Pereira, E.; Vilarigues, M. The Influence of Environment in the Alteration of the Stained-Glass Windows in Portuguese Monuments. *Heritage* **2018**, *1*, 365–376. [[CrossRef](#)]
18. Eastaugh, N.; Walsh, V.; Chaplin, T.; Siddall, R. *Pigment Compendium: A Dictionary of Historical Pigments*; Elsevier Butterworth-Heinemann: Oxford, UK, 2004.
19. *DIN EN ISO 4287; Surface Roughness—Terminology: Part 1, Surface and Its Parameters*. ISO: Geneva, Switzerland, 1998.
20. Ariyathilaka, P.; Haddock, D.; Spindloe, C.; Tolley, M.K. Surface Roughness of NaCl Coating Used as Release Layers in Thin Film Production. *J. Phys. Conf. Ser.* **2018**, *1079*, 012017. [[CrossRef](#)]
21. *ISO 2409; European ISO Standard, Paints, and Varnishes—Cross Cut Test*. ISO: Geneva, Switzerland, 1992.
22. Wolbers, R. *Cleaning Painted Surfaces*; Archetype Publications Ltd.: London, UK, 2000.
23. Redol, P. *O Mosteiro Da Batalha e o Vitral Em Portugal Nos Séculos XV e XVI*; da Batalha, C.M., Ed.; Câmara Municipal da Batalha: Batalha, Portugal, 2003.
24. Eberhard, Z. *Chemische Technologie des Glases*; Cable, M., Translator; Society of Glass Technology: Sheffield, UK, 2013.
25. Schmidt-Whitley, R.D.; Martinez-Clemente, M.; Revcolevschi, A. Growth and Microstructural Control of Single Crystal Cuprous Oxide Cu<sub>2</sub>O. *J. Cryst. Growth* **1974**, *23*, 113–120. [[CrossRef](#)]
26. García-Heras, M.; Carmona, N.; Gil, C.; Villegas, M.A. Neorenaissance/Neobaroque Stained Glass Windows from Madrid: A Characterisation Study on Some Panels Signed by the Maumejean Frères Company. *J. Cult. Herit.* **2005**, *6*, 91–98. [[CrossRef](#)]
27. Beltrán, M.; Schibille, N.; Brock, F.; Gratuze, B.; Vallcorba, O.; Pradell, T. Modernist Enamels: Composition, Microstructure and Stability. *J. Eur. Ceram. Soc.* **2020**, *40*, 1753–1766. [[CrossRef](#)]
28. Beltrán, M.; Schibille, N.; Gratuze, B.; Vallcorba, O.; Bonet, J.; Pradell, T. Composition, Microstructure and Corrosion Mechanisms of Catalan Modernist Enamelled Glass. *J. Eur. Ceram. Soc.* **2021**, *41*, 1707–1719. [[CrossRef](#)]
29. Weber, F.W. *Artists’ Pigments: Their Chemical and Physical Properties*; D. Van Nostrand Company: New York, NY, USA, 1923.
30. Hudson Institute of Mineralogy. Melanotekite (mindat.org). Available online: <https://www.mindat.org/min-2632.html> (accessed on 30 June 2022).
31. Ito, J.; Frondel, C. Syntheses of Lead Silicates: Larsenite, Barysilite and Related Phases. *Am. Mineral.* **1967**, *52*, 1077–1084.
32. Bettembourg, J.-M. Composition et Durabilité Des Grisailles. *Sci. Technol. Conserv. Restaur. Oeuvres d’Art Patrim.* **1991**, *2*, 47–55.
33. Silvestri, A.; Molin, G.; Pomero, V. The Stained Glass Window of the Southern Transept of St. Anthony’s Basilica (Padova, Italy): Study of Glasses and Grisaille Paint Layers. *Spectrochim. Acta Part B At. Spectrosc.* **2011**, *66*, 81–87.

34. Machado, C.; Vilarigues, M.; Palomar, T. Characterization of the Alteration of Debitus Grisailles. *Stud. Conserv.* **2021**, *67*, 413–422. [[CrossRef](#)]
35. Cílová, Z.Z.; Kučerová, I.; Knížová, M.; Trojek, T. Corrosion Damage and Chemical Composition of Czech Stained Glass from 13th to 15th Century. *Glass Technol. Eur. J. Glass Sci. Technol. Part A* **2015**, *56*, 153–162.
36. Palomar, T. Chemical Composition and Alteration Processes of Glasses from the Cathedral of León (Spain). *Bol. la Soc. Esp. Ceram. Vidr.* **2018**, *57*, 101–111. [[CrossRef](#)]
37. Shrimali, K.; Jin, J.; Hassas, B.V.; Wang, X.; Miller, J.D. The Surface State of Hematite and Its Wetting Characteristics. *J. Colloid Interface Sci.* **2016**, *477*, 16–24. [[CrossRef](#)]